PAPER

Check for updates

Anticancer and antimicrobial properties of novel η6-*p*-cymene ruthenium(II) complexes containing a N,S-type ligand, their structural and theoretical characterization†

Ewelina Namiecińska,[a] Beata Sadowska,[b] Marzena Więckowska-Szakiel,[b] Anna Dołęga, [ID][c] Beata Pasternak,[d] Magdalena Grazul[e] and Elzbieta Budzisz [ID] *[a]

Ruthenium(II) complexes are lately of great scientific interest due to their chemotherapeutic potential as anticancer and antimicrobial agents. Here we present the synthesis of new pyrazole carbothioamide derivatives and their four arene–ruthenium complexes. The title compounds were characterized with the application of IR, NMR, mass spectrometry, elemental analysis and X-ray diffraction. Additionally, for new complexes DFT calculations were done. Their antimicrobial activity (MIC, MBC/MFC) was examined *in vitro* against *Staphylococcus aureus*, *Staphylococcus epidermidis*, *Enterococcus faecalis*, *Pseudomonas aeruginosa*, *Proteus vulgaris* and *Candida albicans*. Their cytotoxic effects, using the MTT assay, against three cancer cell lines: HL-60, NALM-6, WM-115 and normal human foreskin fibroblasts (HFF-1) were also investigated. The influence of the new arene–ruthenium(II) complexes on the DNA structure was also tested. From our results, compound **2d** showed higher cytotoxicity against melanoma cell line WM-115 than cisplatin. Strong biostatic and biocidal activity of the tested complexes against Gram-positive bacteria, including *S. aureus*, *S. epidermidis* and *E. faecalis* was demonstrated. The new arene–ruthenium(II) compounds could not only inhibit proliferation of cancer cells, but also protect patients against malignant wound infections.

1. Introduction

The half-sandwich arene–ruthenium(II) complexes with different co-ligands have been recognized as chemotherapeutics agents and promising alternatives to cisplatin and its oxaliplatin analogs.[1,2] Cisplatin was the first metal-ion complex used in chemotherapy, but unfortunately drug resistance and side effects have limited its clinical utility. The ruthenium complexes could be a valuable alternative to cisplatin. Some of the most investigated classes of organometallic compounds are RAPTA-C [(Ru-*p*-cymene)(1.3.5-triaza-7-phosphaadamantane)Cl$_2$], NAMI-A (imidazolium *trans*-[tetrachloro(dimethylsulfoxide)(1*H*-imidazole)ruthenate(III)]), KP1019 (indazolium *trans*-[tetrachlorobis(1*H*-indazole)-ruthenate(III)]) complexes. Currently, most of them are undergoing clinical trials (Scheme 1).[3–6] An arene substituent is relatively inert towards displacement and is known to stabilize ruthenium complexes in the oxidation state +2 under physiological conditions. Corresponding Ru(II) complexes are kinetically similar to Pt(II) complexes.[7] Chelating ligands containing sulfur and nitrogen atoms have been used by many researchers to achieve a limited lability of the complexes, in order to enhance their biological activity. N,S-Ligands coordinate to metal ion center *via* the sulfur atom and the pyridine-like nitrogen of pyrazole moiety with the formation of a stable five-membered ring.[8]

Both the size and hydrophobicity of the coordinated arene substituents as well as the structure of the mono- or bidentate co-ligands have an influence on biological activity of arene–ruthenium(II) complexes.[9] The metal center in arene–ruthenium(II) complexes is pseudotetrahedral. Thus, ligands can occupy maximum three coordination sites. This structural feature of the piano-stool complexes allows to create diverse coordination complexes using a variety of N-, O-, S- and P-donors as ligands. A large number of possibilities of

[a]*Department of Cosmetic Raw Materials Chemistry, Medical University of Lodz, Muszynskiego 1, 90-151 Lodz, Poland. E-mail: elzbieta.budzisz@umed.lodz.pl*

[b]*Department of Immunology and Infectious Biology, Institute of Microbiology, Biotechnology and Immunology, Faculty of Biology and Environmental Protection, University of Lodz, Banacha 12/16, 90-237 Lodz, Poland*

[c]*Department of Inorganic Chemistry, Faculty of Chemistry, Gdansk University of Technology, Narutowicza 11/12, 80-233 Gdansk, Poland*

[d]*Department of Organic Chemistry, Faculty of Chemistry, University of Lodz, Tamka 12, 91-403 Lodz, Poland*

[e]*Department of Pharmaceutical Microbiology and Microbiological Diagnostics, Faculty of Pharmacy, Medical University of Lodz, Pomorska 137 Street, 90-235 Lodz, Poland*

† Electronic supplementary information (ESI) available. CCDC 1896357–1896360. For ESI and crystallographic data in CIF or other electronic format see DOI: 10.1039/c9ra08736b
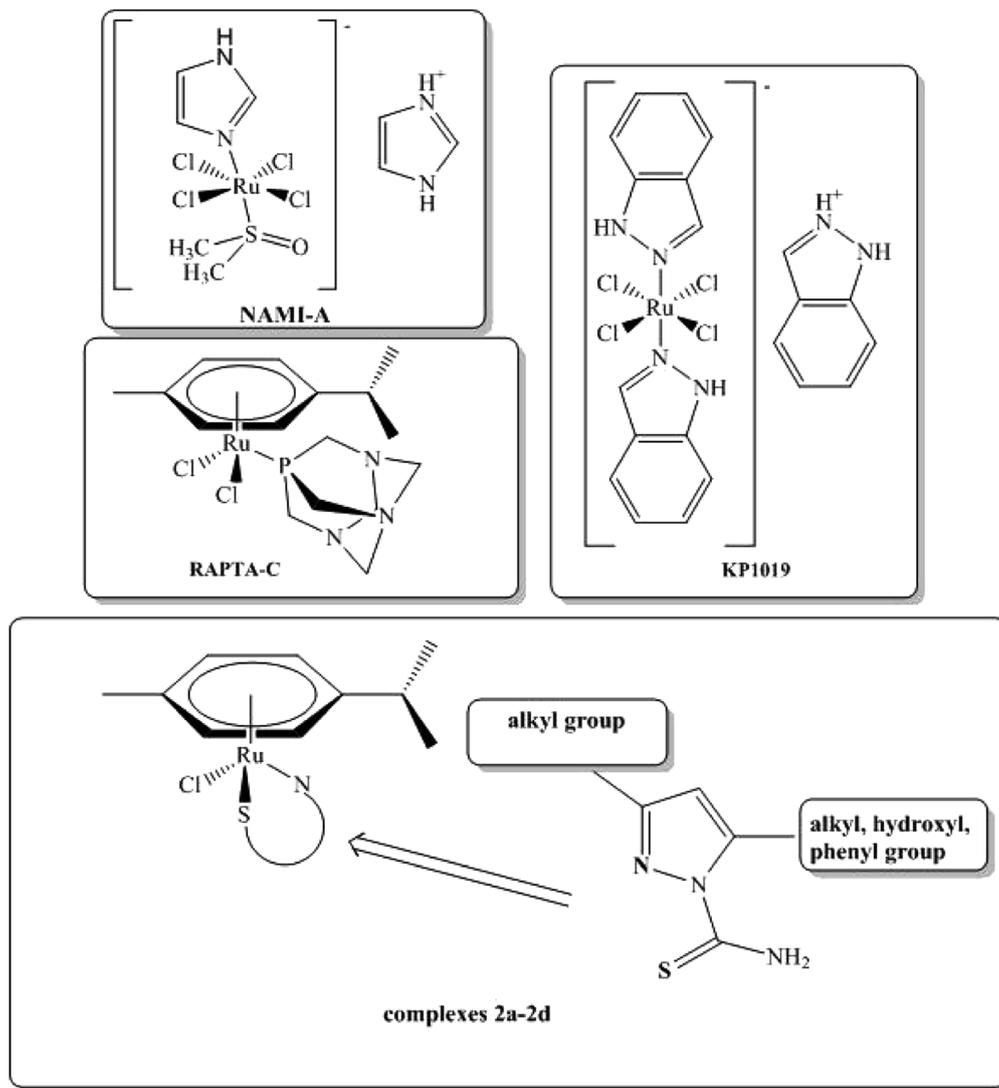
Scheme 1 Structures of anticancer NAMI-A, KP1019, RAPTA-C compounds and newly synthesized **2a–2d** complexes.

coordination allows to manipulate pharmacological properties of half-sandwich arene–Ru(II) complexes making them ideal candidates for preparing multifunctional drugs.[10,11]

Pyrazole and its derivatives demonstrate various biological activities, *e.g.* antibacterial, antifungal, antiviral, anticancer, anticonvulsant, analgesic, anti-inflammatory, anti-diabetic, sedative, anti-rheumatic. Moreover, they are applied as dyes and agrochemicals.[12–16] So far, scientific interest has been focused mainly on the anticancer activity of the complexes of pyrazole carbothioamide derivatives with various metal ions, *e.g.* Cu(II), Zn(II), Co(II) and Ni(II) against HL-60, NALM-6, WM-15 and HUVECs cell lines.[17–20] It is widely known that melanoma is one of the most difficult diseases to cure due to its high resistance to anticancer drugs. It has been proved that arene–ruthenium(II) complexes display anti-melanoma activity, which is probably based on their interference with mTOR and independent from EGFR (epidermal growth factor receptors) inhibition.

Due to the fact that human microbiome plays an important role not only by providing proper functions of skin and mucous membrane barriers, but also in the etiology of many pathological processes (*e.g.* wound infections, cancer, ulcerations), the antimicrobial activity of potential anticancer drugs should be tested. Wound infections are quite common in patients with cancer, especially with breast, head, neck or melanoma cancers. Interestingly, it has been proved that metal complexes have antimicrobial effect; therefore their application on the skin could diminish the development of melanoma cells and at the same time protect against wound infections. Anyway, it has to be pointed out that the power of antimicrobial activity of such compounds strongly depends on their structure and composition. Thus, it is a good practice to test antimicrobial activity of each new anticancer drug.

The aim of this study was to synthesize new arene–ruthenium(II) complexes with selected pyrazole derivatives and to evaluate their anticancer and antimicrobial activity. All the

complexes were obtained in reactions between ligands containing various substituents (methyl, ethyl, carbonyl, phenyl) in C-3 and C-5 position of the pyrazole ring and [RuCl$_2$(p-cymene)$_2$]$_2$ dimer. Next, they were characterized with the use of several physico-chemical methods, including X-ray diffraction and DFT calculations.

2. Experimental

2.1. Materials and methods

All starting reagents: [RuCl$_2$(p-cymene)$_2$]$_2$ dimer, anhydrous solvents: dichloromethane, isopropyl alcohol, diethyl ether were purchased from Sigma-Aldrich and Avantor Performance and they were commercially available. Synthesis of complexes was carried out in the argon atmosphere conditions using Schlenk techniques. Ligands **1a**, **1c** and **1d** were prepared with the use of methods described before.[20,23,24] The ^{1}H NMR and ^{13}C NMR spectra were registered in DMSO-d[6] (for all complexes) and CDCl$_3$-d (for ligand **1b**) using Bruker Avance III 600 MHz spectrometer. The IR spectra were recorded in KBr on the FTIR-8400S Shimadzu Spectrophotometer. The ESI-MS spectra were measured on Varian 500-MS LC Ion Trap. An elemental analysis was performed at the Faculty of Chemistry (University of Lodz) using a Vario Micro Cube by Elemental analyzer. Melting points of all compounds were determined in open capillary tubes on Büchii apparatus B-540 and were uncorrected. Anticancer activity was tested against three cancer cell lines: HL-60, NALM-6 and WM-115 in the Department of Bioorganic Chemistry at the Medical University of Lodz (anticancer), while antimicrobial activity was carried out on selected bacteria and fungi strains were done in the Department of Immunology and Infectious Biology at the University of Lodz. The MTT method was used to determine cells viability.

2.2. Synthetic procedures

Synthesis of ligand 1-[amino(thioxo)methyl]-3,5-dimethyl-1H-pyrazole (**1a**), 1-[amino(thioxo)methyl]-5-hydroxy-3-phenyl-1H-pyrazole (**1c**) and 1-[amino(thioxo)methyl]-5-hydroxy-3-methyl-1H-pyrazole (**1d**) was executed as described before (Sobiesiak et al. and Grazul et al.)[20,23,24] with some modifications.

2.2.1. Synthesis of 1-[amino(thioxo)methyl]-3,5-diethyl-1H-pyrazole (1b). The 3,5-diethyl-1H-pyrazole-1-carbothioamide was prepared according to literature.[20,23] Hydrazinocarbothioamide (1.25 g, 0.014 mol) was dissolved in 80 ml (0.2 M) hydrochloric acid solution. Next, heptane-2,4-dione was added to the stirred mixture. The reaction was stirred at room temperature for 4 h. Next, white precipitation was filtered off. The last step of the reaction involved washing the white precipitation with water and drying it under reduced pressure. Yield: (1.74 g, 69.2%), mp dec. > 128.0 °C. FTIR (KBr cm^{-1}): ν (N–H) 3388, 3235; ν (C–H) 3123; ν (CH$_3$CH$_2$–) 2969, 2921, 2871; ν (C=N) 1594, 1571; ν (C–N) 1368; ν (N–N) 1026; ν (C=S) 886. Elemental analysis for C$_8$H$_{13}$N$_3$S: C 52.42(52.35), H 7.15(7.17), N 22.93(22.99), S 17.50(17.42). ^{1}H NMR (600 MHz, CDCl$_3$-d) δ (ppm): 1.22 (t, 3H, –CH$_2$**CH$_3$**, $^3J_{HH}$ = 6.0 Hz), 1.27 (t, 3H, –CH$_2$**CH$_3$**, $^3J_{HH}$ = 6.0 Hz), 2.57 (q, 2H, $^3J_{HH}$ = 6.0 Hz, –**CH$_2$**CH$_3$),

3.27 (q, 2H, $^3J_{HH}$ = 6.0 Hz –**CH$_2$**CH$_3$), 6.07 (s, 1H, –CH pyrazole), 7.01, 8.64 (2 br. s., 2H, **NH$_2$**).^{13}C NMR (600 MHz, CDCl$_3$-d) δ (ppm): 179.4 (C=S), 155.6, 152.50 (2C pyrazole), 109.0 (CH pyrazole), 24.33, 21.45 (2CH$_2$), 12.80, 12.77 (2CH$_3$). ESI-MS (m/z): 182.1 (100%); 184.1(25%).

2.2.2. Synthesis of arene–ruthenium(II) complexes (2a–2d). The arene–ruthenium(II) complexes (**2a–2d**) with carbothioamidopyrazole derivatives were obtained from pyrazole derivatives with various substituent in C-3- and C-5-ring position, containing thiosemicarbazide motive (–CSNH$_2$).

2.2.2.1. Synthesis of [(η[6]-p-cymene)Ru(1-[amino(thioxo)methyl]-3,5-dimethyl-1H-pyrazole)Cl$_2$ (2a). The solution of 1-[amino(thioxo)methyl]-3,5-dimethyl-1H-pyrazole (47.50 mg, 0.3 mmol) in 6 ml of dry anhydrous dichloromethane was dropped slowly to the solution of dichloro(p-cymene)ruthenium(II)dimer (92.06 mg, 0.15 mmol) in 5 ml of dry anhydrous dichloromethane. Next, the mixture was stirred out under atmospheric argon condition at room temperature in Schlenk tube. After 24 hour heating, the mixture was concentrated under reduced pressure and then diethyl ether was added. The precipitation was filtered off as orange solid. Single crystals of **2a** for X-ray analysis were obtained from recrystallization of precipitated product (diffusion method in solvents system: dichloromethane/hexane) Yield: (127.76 mg, 88.83%), orange crystals, mp 131.5–132.3 °C. FTIR (KBr cm^{-1}): ν (N–H) 3379; ν (C=N) 1622; ν (C=C) 1470; ν (C–N) 1353; ν (C–H) 1157; ν (N–N) 1052, ν (C=S) 872. Anal. calcd for C$_{16}$H$_{24}$ClN$_3$SRu 0.5CH$_2$Cl$_2$ (M = 479.42 g mol^{-1}): C 40.93 (40.96), H 5.15 (5.55), N 8.95(8.97), S 6.83(6.85). ^{1}H NMR (600 MHz, DMSO-d[6]) δ (ppm): 1.02, 1.15 (2d, $^3J_{HH}$ = 12.0 Hz, 6H, CH(**CH$_3$**)$_2$ p-cymene), 2.08 (s, 3H, CH$_3$ p-cymene), 2.62 (septet, $^3J_{HH}$ = 6.0 Hz, 1H, **CH**(CH$_3$)$_2$ p-cymene), 2.70 (2 s, 6H, 2CH$_3$ pyrazole), 5.70, 6.05, 6.12, 6.16 (4d, $^3J_{HH}$ = 6.0 Hz, 4Ar CH), 6.70 (s, 1H, CH pyrazole), 9.15 (s, 1H, –NH), 11.41 (s, 1H, –SH pyrazole). ^{13}C NMR (600 MHz, DMSO-d[6]) δ (ppm): 14.22, 17.11, 18.35, 18.73, 21.60 (5CH$_3$), 23.11 (CH), 30.90 (CH pyrazole), 80.95, 83.14, 85.98, 86.83, 86.95, 87.84 (6CHAr p-cymene), 115.33(C–NH), 145.70 (C=S). ESI-MS (m/z): 423.1(42%) 425.0(69%) 426.1(100%) 427.1(36%) 428.0(76%).

2.2.2.2. Synthesis of [(η[6]-p-cymene)Ru(1-[amino(thioxo)methyl]-3,5-diethyl-1H-pyrazole)Cl$_2$ (2b). The solution of 1-[amino(thioxo)methyl]-3,5-diethyl-1H-pyrazole (55.0 mg, 0.3 mmol) in 6 ml of dry anhydrous isopropanol and 3 ml anhydrous dichloromethane was dropped slowly to the solution of dichloro(p-cymene)ruthenium(II)dimer (92.0 mg, 0.15 mmol) in 5 ml of dry anhydrous dichloromethane. Next, the mixture was stirred under atmospheric argon at room temperature in Schlenk tube. After 24 h of heating, the mixture was concentrated under reduced pressure and then diethyl ether was added. The precipitation was filtered as orange solid. Single crystals of **2b** from X-ray analysis were obtained from recrystallization of precipitated product (diffusion method in solvents system: dichloromethane/hexane). Yield: (109.79 mg, 82.1%), orange crystals, mp 147.9–148.6 °C. FTIR (KBr cm^{-1}): ν (N–H) 3417; ν (C=N) 1606; 1486 ν (C=C) 1470; ν (C–N) 1363; ν (C–H) 1166; ν (N–N) 1046, ν (C=S) 872. Anal. calcd for C$_{18}$H$_{27}$ClN$_3$SRu (M = 496.51 g mol^{-1}): C 43.63(43.60), H 5.29(5.64), N 8.48(8.16), S 6.47(7.03).

^{1}HNMR (600 MHz, DMSO-d^6) δ (ppm): 1.04, 1.17 (2d, $^3J_{HH}$ = 6.0 Hz, 6H, CH(**CH$_3$**)$_2$), 1.26, 1.37 (2t, $^3J_{HH}$ = 18.0 Hz, 6H, **CH$_2$CH$_3$**), 2.16 (s, 3H, CH$_3$ *p*-cymene), 2.62 (septet, $^3J_{HH}$ = 6.0 Hz, 1H, **CH**(CH$_3$)$_2$), 3.16 (m, 4H, **CH$_2$CH$_3$**), 5.72, 6.04, 6.14, 6.19 (4d, $^3J_{HH}$ = 6.0 Hz, 4Ar CH), 6.84 (s, CH pyrazole), 11.40 (s, 1H, –NH pyrazole).^{13}C NMR (600 MHz, DMSO-d^6) δ (ppm): 11.83, 12.94, 18.29, 18.76, 21.21, 21.44, 23.05 (7CH$_3$), 24.30 (CH), 30.86 (CH pyrazole), 81.03, 83.27, 86.01, 86.81, 87.28, 88.08 (CHAr *p*-cymene), 111.11(C–NH), 152.01 (C=S). ESI-MS (*m/z*): 415.1(45%) 416.1(49%) 417.1(59%) 418.1(100%) 419.1(33%) 420.0(74%).

2.2.2.3. Synthesis of [(η^6-p-cymene)Ru(1-[amino(thioxo)methyl] -5-hydroxy-3-phenyl-1H-pyrazole)Cl$_2$ (2c). The solution of 1-[amino(thioxo)methyl]-5-hydroxy-3-phenyl-1*H*-pyrazole (67.52 mg, 0.3 mmol) in 8 ml of dry anhydrous dichloromethane and 2.5 ml anhydrous isopropanol was dropped slowly to the solution of dichloro(*p*-cymene)ruthenium(II)dimer (92.46 mg, 0.15 mmol) in 6 ml of dry anhydrous dichloromethane. Next, the mixture was stirred under atmospheric argon at room temperature in Schlenk tube. After 24 h of heating, the mixture was concentrated under reduced pressure and then diethyl ether was added. The precipitation was filtered off as orange solid. Single crystals of **2c** for X-ray analysis were obtained from recrystallization of precipitated product (diffusion method in solvents system: dichloromethane/hexane). Yield: (137.31 mg, 84.29%), bright orange crystals, mp (dec. > 274 °C). FTIR (KBr cm^{-1}): ν (OH) 3237; ν (N–H) 3072; ν (C=N) 1651; ν (C=O) 1609; 1458 (C=C) 1470; ν (C–N) 1391; ν (N–N) 1087, ν (C=S) 872. Anal. calcd for C$_{20}$H$_{25}$ClN$_3$OSRu·1.3H$_2$O (M = 528.5 g mol^{-1}) C 45.45(45.92), H 4.73 (4.93), N 7.95(7.93), S 6.06(5.34).^{1}H NMR (600 MHz, DMSO-d^6) δ (ppm): 0.93, 1.00 (2d, $^3J_{HH}$ = 6.0 Hz, CH(**CH$_3$**)$_2$), 2.76 (s, CH$_3$ *p*-cymene), 2.43 (septet, $^3J_{HH}$ = 6.0 Hz, **CH**(CH$_3$)$_2$), 4.71, 4.80, 5.13, 5.63 (4d, $^3J_{HH}$ = 6.0 Hz, 4Ar CH), 5.20 (s, CH pyrazole), 7.65 (m, 3H Ar CH), 8.02 (m, 2H Ar CH), 10.35 (s, 1H, –OH pyrazole), 10.80 (s, 1H, –NH pyrazole). ^{13}C NMR (600 MHz, DMSO-d^6) δ (ppm): 18.64, 21.24, 21.91, 22.97 (4CH$_3$), 30.54 (CH *p*-cymene), 80.46, 83.36, 85.64, 85.86, 86.37, 87.93 (12CHAr), 100.47 (CH), 66.94 (C=O), 165.83(C–NH), 175.88 (C=S). ESI-MS (*m/z*): 451.1(42%) 452.2(39%) 453.1(63%) 454.1(100%) 456.0(60%).

2.2.2.4. Synthesis of [(η^6-p-cymene)Ru(1-[amino(thioxo) methyl]-5-hydroxy-3-methyl-1H-pyrazole) Cl$_2$ (2d). The solution of 1-[amino(thioxo)methyl]-5-hydroxy-3-methyl-1*H*-pyrazole (48.14 mg, 0.3 mmol) in 8 ml of dry anhydrous dichloromethane was dropped slowly to the solution of dichloro(*p*-cymene)ruthenium(II)dimer (92.03 mg, 0.15 mmol) in 6 ml of dry anhydrous dichloromethane. Obtained mixture was stirred out under atmospheric argon at room temperature in Schlenk tube. After 24 h of heating, the mixture was concentrated under reduced pressure and then diethyl ether was added. The precipitation was filtered off as brown solid. Single crystals of **2d** for X-ray analysis were obtained from recrystallization of precipitated product (method in solvents system in methanol). Yield: (146.98 mg, 92.71%), brown crystals, mp 144.3–145.8 °C. FTIR (KBr cm^{-1}): ν (NH$_2$) 3459, 3367; ν (OH) 3240; ν (C=O) 1603; ν (C=C) 1492, 1477; ν (C–N) 1397, ν (N–N) 1021; ν (C=S) 891. Anal. calcd for C$_{15}$H$_{22}$ClN$_3$O$_2$SRu·H$_2$O (M = 491.39 g mol^{-1}) C

36.66(36.09), H 4.51(4.84), N 8.55(8.26), S 6.53(6.22). ^{1}H NMR (600 MHz, DMSO-d^6) δ (ppm): 0.98, 1.03 (2d, $^3J_{HH}$ = 6.0 Hz, 6H, CH(**CH$_3$**)$_2$), 2.07 (s, CH$_3$), 2.37 (s, CH$_3$ pyrazole), 2.55 (septet, $^3J_{HH}$ = 6.0 Hz, **CH**(CH$_3$)$_2$), 5.50, 5.83, 5.89, 5.92 (4d, $^3J_{HH}$ = 6.0 Hz, 4H Ar CH), 10.13 (s, 1H, OH), 10.56 (s, 1H, NH). ^{13}C NMR (600 MHz, DMSO-d^6) δ (ppm): 15.59, 16.69, 17.67, 18.62 (4CH$_3$), 25.54 (C pyrazole), 31.02 (CH *p*-cymene), 65.82 (CH pyrazole), 80.35, 82.92, 84.61, 85.89, 86.10, 87.49 (6CHAr), 161.68 (C=O), 165.24 (C–NH), 175.18 (C=S). ESI-MS (*m/z*): 389.1(34%) 390.1(38%) 394.1(52%) 392.1(100%) 394.1(54%).

2.3. Crystal structure determination

Single crystal X-ray diffraction data of compounds **2a**, **2b**, **2c** and **2d** were collected on a Stoe IPDS-2T diffractometer with graphite-monochromated Mo-Kα radiation; crystals were cooled using a Cryostream 800 open flow nitrogen cryostat (Oxford Cryosystems). Data collection and image processing were performed with X-Area 1.75.[46] Intensity data were scaled with LANA (the part of X-Area) in order to minimize different intensities of symmetry-equivalent reflections (the multi-scan method).

Structures were solved by direct methods and all non-hydrogen atoms were refined with anisotropic thermal parameters by full-matrix least squares procedure based on F2 using the SHELX-2014 program package.[47] The Olex[48] and Wingx[49] program suites were used to prepare the final cif files. Figures were prepared with the freeware Mercury 4.0.0.[50] Hydrogen atoms were usually refined using isotropic model with Uiso(H) values fixed to be 1.5 times $U_{eq.}$ of C atoms for –CH$_3$ or 1.2 times $U_{eq.}$ for –CH$_2$ and –CH groups. Disordered molecule of dichloromethane, present in the crystals of compound **2a**, was refined as disordered between two positions with occupation factors 0.59(3)/0.41(3). Crystal parameters and refinement details are collected in Table 1.

Crystallographic data for the structural analysis has been deposited with the Cambridge Crystallographic Data Center, no. CCDC 1896357 **2a**, CCDC 1896358 **2b**, CCDC 1896359 **2c**, CCDC 1896360 **2d**.

2.4. Minimal inhibitory, bactericidal/fungicidal concentration (MIC, MBC/MFC)

The MIC of arene–ruthenium(II) complexes with carbothioamidopyrazole derivatives **2a–2d**, as well as the ligands alone **1a–1d** and dimer, tested at a final concentration range of 31.2–1000 μg ml^{-1}, were determined by the broth microdilution method, according to the EUCAST guidelines.[51] Stock solutions of the lyophilized compounds (80 mg ml^{-1}) were freshly prepared in 100% DMSO (POCh, Poland) and further diluted in liquid culture medium (Mueller-Hinton Broth (BTL, Poland) for bacteria; RPMI-1640 without phenol red (Sigma, USA) for fungi). The highest concentration of the solvent never exceeded 1.25% in order not to limit viability of the microbes. Briefly, MIC was defined as the lowest concentration of the compounds inhibiting bacterial/fungal growth after 24–48 h of co-incubation at 37 °C compared to the appropriate positive controls. The microorganisms in culture medium containing DMSO at the highest final concentration (1.25% vol/vol) served as positive

Table 1 Crystal data and structure refinement for **2a–2d**

Identification code	2a	2b	2c	2d
Empirical formula	$C_{17}H_{25}Cl_4N_3RuS$	$C_{18}H_{27}Cl_2N_3RuS$	$C_{20}H_{22}ClN_3ORuS$	$C_{15}H_{22}ClN_3O_2RuS$
Formula weight [u]	546.33	489.45	488.98	444.93
Temperature [K]	120(2)			
Wavelength [Å]	0.71073			
Crystal system	Orthorhombic	Orthorhombic	Monoclinic	Orthorhombic
Space group	$Pbca$	$Pbca$	$P2_1/c$	$P2_12_12_1$
Unit cell dimensions				
a [Å]	13.077(7)	10.6918(18)	10.6196(18)	10.398(2)
b [Å]	14.235(6)	14.539(2)	12.7321(17)	12.551(3)
c [Å]	23.698(10)	26.597(4)	14.8584(15)	13.766(5)
α [°]	90	90	90	90
β [°]	90	90	107.980(11)	90
γ [°]	90	90	90	90
Volume [Å³]	4412(4)	4134.5(11)	1910.9(5)	1796.6(8)
Z	8	8	4	4
Density (calcd.) [mg m⁻³]	1.645	1.573	1.700	1.645
Absorption coefficient [mm⁻¹]	1.297	1.124	1.085	1.149
Absorption corr. method	Integration			
$F(000)$	2208	2000	992	904
Crystal size [mm]	0.132 × 0.092 × 0.059	0.107 × 0.073 × 0.033	0.075 × 0.059 × 0.029	0.095 × 0.077 × 0.044
θ range for data collect [°]	2.283 to 25.998	2.444 to 25.999	3.200 to 25.999	2.943 to 25.995
Reflections collected	15 362	20 018	9994	10 472
Independent reflections	4273	4043	3737	3509
$R(\text{int})$	0.1075	0.0398	0.0531	0.0678
Completeness to $\theta = 25.242°$	0.985	0.995	0.994	0.994
Data/restraints/parameters	4273/2/268	4043/0/239	3737/0/247	3509/0/216
Goodness-of-fit on F^2	1.082	1.040	1.019	1.037
Final R indices [$I > 2\text{sigma}(I)$]	$R_1 = 0.0816$	$R_1 = 0.0284$	$R_1 = 0.0400$	$R_1 = 0.0441$
	$wR_2 = 0.1567$	$wR_2 = 0.0563$	$wR_2 = 0.0776$	$wR_2 = 0.0829$
R indices (all data)	$R_1 = 0.1343$	$R_1 = 0.0426$	$R_1 = 0.0672$	$R_1 = 0.0655$
	$wR_2 = 0.1763$	$wR_2 = 0.0610$	$wR_2 = 0.0860$	$wR_2 = 0.0906$
Largest diff. peak/hole [e Å⁻³]	0.945 and −1.521	0.438 and −0.481	0.561 and −0.730	0.556 and −0.588

controls. The lowest concentration of the preparations that prevented growth of the bacteria or yeast after subculturing 10 μl from the wells marked as MIC, 2× MIC and 4× MIC on solid (agar) medium (incubation for 24 h at 37 °C) was interpreted as MBC/MFC. Experiments were carried out in duplicate in each of 2 separate sets of experiments.

2.5. Cytotoxic activity on human foreskin fibroblasts HFF-1

Cytotoxicity of the compounds was tested on human foreskin fibroblasts HFF-1 (ATCC-SCRC-1041) (LGC Standards Sp. z o.o., Poland) using the 3-(4,5-dimethylthiazol-2-yl)-2,5-diphenyltetrazolium bromide (MTT) reduction assay. Briefly, HFF-1 were seeded 1×10^5 per well on 96-well plates (Nunc, Denmark) in DMEM (Sigma, USA) with 15% (v/v) fetal calf serum (FCS; Cytogen, Poland) and 1% (v/v) penicillin/streptomycin (Sigma, USA) and cultured for 48 h at 37 °C, 5% CO_2. Stock solutions of the lyophilized compounds (25 mM) were freshly prepared in 100% DMSO (POCh, Poland) and further diluted in cell culture medium to obtain the final concentration range of 3.9–500 μM. The final concentration of DMSO did not exceed 2%, *i.e.* the value that did not affect viability of eukaryotic cells. The cells in culture medium containing DMSO (2% v/v) served as positive control (100% of cells viability). HFF-1 were exposed to arene–ruthenium(II)

complexes, ligands and dimer for 24 h under the above culture conditions. The supernatants were removed, the cells were washed and next, 100 μl fresh culture medium and 50 μl MTT (1.5 mg ml⁻¹ in PBS; Sigma, USA) was added and the incubation was continued for 2 h. After the aspiration of the MTT-containing medium, 100 μl of 20% sodium dodecylsulfate (SDS; Sigma, USA) in the mixture of dimethylforamide (DMF) with water (1 : 1) was added to dissolve blue formazan crystals produced by metabolically active cells. After overnight incubation at room temperature, the absorbance was read ($\lambda = 550$ nm) using multifunctional plate reader Victor2 (Wallac, Finland) and compared with positive control to calculate the percentage of cell viability and the IC_{50} (concentration contributing to 50% loss of viability). IC_{50} were calculated based on curve equations determined for the lines of trends the cell viability dependence on tested compounds concentration. Two independent experiments with two replicates in each were performed.

2.6. Anticancer activity of ligands and their complexes 2a–2d

Cytotoxicity of all ligands and their complexes was tested against human leukemia promyelocytic HL-60, lymphoblastic NALM-6 and human skin melanoma WM-115 cell lines. Carboplatin and cisplatin were used as a reference. The cytotoxic

effect was determined using MTT [3-(4,5-dimethylthiazol-2-yl)-2,5-diphenyltetrazolium bromide, Sigma-Aldrich, St. Louis, MO] assay as described before. All tested compounds were incubated with tested cell lines for 46 h. Next, cells were treated with the MTT reagent and incubation was continued for another 2 h. IC_{50} values (expressed as the concentration of the tested compound required to reduce the cells survival fraction to 50% of the control) were calculated from concentration–response curves. Stock solutions of the tested compounds (**1a–1d**, **2a–2d**, dimer, carboplatin and cisplatin) were every time freshly prepared in DMSO solvent. All ligands **1a–1d** were diluted in complete culture medium to final concentration 10^{-7} to 10^{-3} M, while arene Ru(II)complexes **2a–2d** were diluted to final concentration 10^{-7} to 10^{-4} M. In these assay, DMSO concentration never exceeded 0.2% and had no influence on cell growth. Moreover, cultured cells that grew in the absence of drugs were used as a control.

2.7. Cleavage of pUC57 DNA

The DNA cleavage ability of the ruthenium(II) complexes was studied by using agarose gel electrophoresis. Supercoiled plasmid pUC57 DNA (4634bp), dissolved in 10 mM Tris–HCl 50 mM NaCl buffer (pH 7.2), was treated with tested compounds (50, 100, 200, 300 and 400 μM). All mixtures were incubated at 37 °C for 24 h and then the loading buffer (1 μl) containing 25% bromophenol blue, 0.25% xylene cyanol and 30% glycerol, was added.

Each sample (10 μl) was loaded into 1% w/v agarose gel. Electrophoresis was performed at 75 V in Tris–acetate–EDTA (TAE) buffer. The gel was stained with Midori green advance and then photographed under UV light. The proportion of DNA in each fraction was quantitatively estimated from the intensity of each band with the Syngen BTX-20.M system using the Scion Image software. All experiments were carried out in triplicate under the same conditions.

2.8. DFT calculations

DFT calculations *i.e.* geometry optimization, were performed using ADF program (version 2018.01)[52–54] with BP86-D potential and TZP basis in SCF model as implemented in ADF.[55–57] All calculations were performed *in vacuo*.

3. Results and discussion

3.1. Synthesis of compounds

All ligands **1a–1d** can be obtained in reactions of thiosemicarbazide derivatives with appropriate diketones or ketoesters. Cyclic pyrazole-bearing compounds with the carbothioamide group may exist as several tautomeric forms (Scheme 2).[21]

Carbothioamidopyrazoles **1a–1d** possess three potential coordination sites: the nitrogen atom of the pyrazole ring, as well as the nitrogen and sulfur atoms of the thioamide group. Each ligand may act as a neutral, bi- or monodentate moiety.[22] In our experiments, all ligands bind to the ruthenium(II) ion as bidentate N,S-donors to form the corresponding complexes **2a–**

2d. All complexes were synthesized in the reaction between a dichloro(*p*-cymene)ruthenium(II)dimer (**3**) and appropriate carbothioamidopyrazoles containing various substituents in C-3 and C-5 position of pyrazole ring: dimethyl substituent (for complex **2a**), diethyl (for complex **2b**), phenyl/methyl and carbonyl or hydroxyl group (for complexes **2c/2d**). All reactions were executed with ligand : metal molar ratio (L : M) 2 : 1 and the reactions for complex **2a** and **2b** were carried out in anhydrous dicholoromethane, used as a solvent (Scheme 3).

In other reactions, the anhydrous dichloromethane and isopropyl alcohol were used as a solvent for complexes **2c** and **2d**. All reactions were carried out at room temperature. Complexes **2a–2d** were obtained as colored powders or solids. Compounds **2a–2d** were structurally characterized with the use of the single crystal X-ray diffraction analysis.

3.2. Characterization of ligand 1b and half-sandwich complexes 2a–2d

3.2.1. The selected spectroscopic methods. The ^{1}H NMR and ^{13}C NMR spectra data were recorded in DMSO-d_6 (for all complexes **2a–2d**) and for new ligand **1b** in CDCl$_3$-d and IR spectra in KBr, as described in the Experimental section. The ^{1}H NMR, ^{13}C NMR, IR spectrals data was obtained for all new complexes **2a–2d** and new ligand **1b**, while ligands **1a**, **1c** and **1d** were prepared by methods described in literature.[20,23,24] The chemical shifts and intensities are compatible with products obtained in the synthesis procedure. Aromatic protons of *p*-cymene were seen in the range from 4.71 to 6.16 ppm as doublets. All complexes showed signals ranging from 5.20 to 6.84 ppm for the proton in the pyrazole ring. The absorption bands characteristic for stretching vibrations of the pyrazole ν(C=N) group were observed shifted to 1594 cm^{-1} and 1571 cm^{-1} (for ligands) and to higher regions stretching from 1606 to 1651 cm^{-1} (for all complexes). Complexes of amino group protons in NMR spectra gave signals from 9.15 ppm to 11.40 ppm. The characteristic bands in IR spectra were assigned a range from 3273 cm^{-1} to 3459 cm^{-1} of the amino group of complexes **2a–2d**. The ^{13}C NMR resonance of the C=S group gave signals for complexes **2a–2d** 145.70, 152.01, 175.88 and 175.18 ppm, respectively. Important signal ν(C=S) for complexes showed stretching vibrations to 872 cm^{-1} (for compounds **2a–2c**), 891 cm^{-1} (for compound **2d**), while for ligand they were shifted to 886 cm^{-1}. It may suggest that sulfur atom in substituents C=S can be a possible site of metal coordination.

3.2.3. Electrospray mass spectroscopy ESI-MS. Electrospray ionization mass spectrometry is a very useful tool for an analysis of different metal complexes because it very well reflects species present in the solution. Successful results can be obtained even for ruthenium complexes if an appropriate solvent is used. The aim of our research was to confirm the structures of the ruthenium complexes **2a–2d** and ligand **1b**. All tested compounds were dissolved in methanol and/or isopropanol. All obtained results are presented in Table 2. Four ruthenium complexes, detected as single-charged cations under the experimental conditions signals.
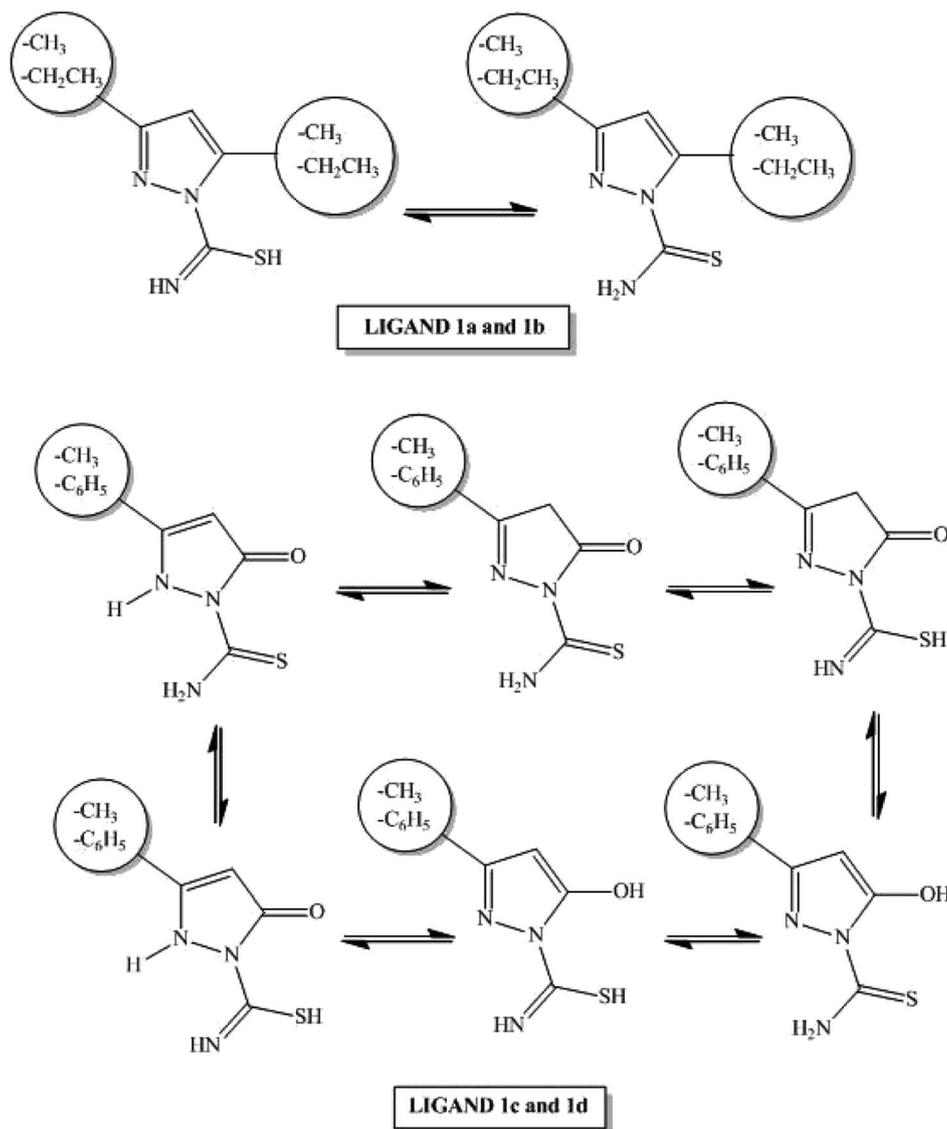
Scheme 2 Tautomeric forms of ligands **1a–1d**.

Therefore, signals of positive and negative ions were observed only for compound **2c**.

Various types of ions were observed for all tested compounds. The most intense signals were obtained for ions, created after losing one or two chlorine atoms. Simulated isotope patterns for **2a** with the chemical formula $[C_{16}H_{23}Cl_2-N_3SRu]^+$ cations exactly matched the mass spectra of complexes **2b**, which means that ionization of these compounds took place *via* the loss of chloride ions. Relevant charts and scan of their mass spectrum are provided in ESI (Fig. 1S†). Very interesting signals were observed at around 815 Da for complex **2a** and around 783 Da for complex **2d**. It was found that these compounds can exist as a complex of two ligands or two complexes. According to literature, this is a common feature for half-sandwich Ru(II) complexes, where ruthenium is connected to the electronegative substituents. Examples are shown in Fig. 2S in ESI.†[25]

The tandem analysis was performed for ions with the highest abundance. All ions $[XRuLCl]^+$, during the first step, eliminate fragments of hydrogen chloride. Further fragments of ms^3 led to leaving HN = C = S (59 Da). Similar effects were observed for ligand (**1b**). The molecule of thiocyanate molecule was easily eliminated. The presented analysis of ESI-MS spectra shows that used compounds are stable in the solutions and it is difficult to break ruthenium–sulfur coordination bonds or permanent nitrogen in tandem reactions even at 200 eV voltage on the capillary and 5000 eV on the needle.

3.3. Crystal structures

The molecular structures of the complexes are illustrated in Fig. 1. Important bond lengths and angles are collected in Table 3. As it was shown in Scheme 3, two types of ruthenium complexes can be distinguished among the compounds – two ionic **2a**, **2b** and two molecular species **2c**, **2d**. The Ru(II)
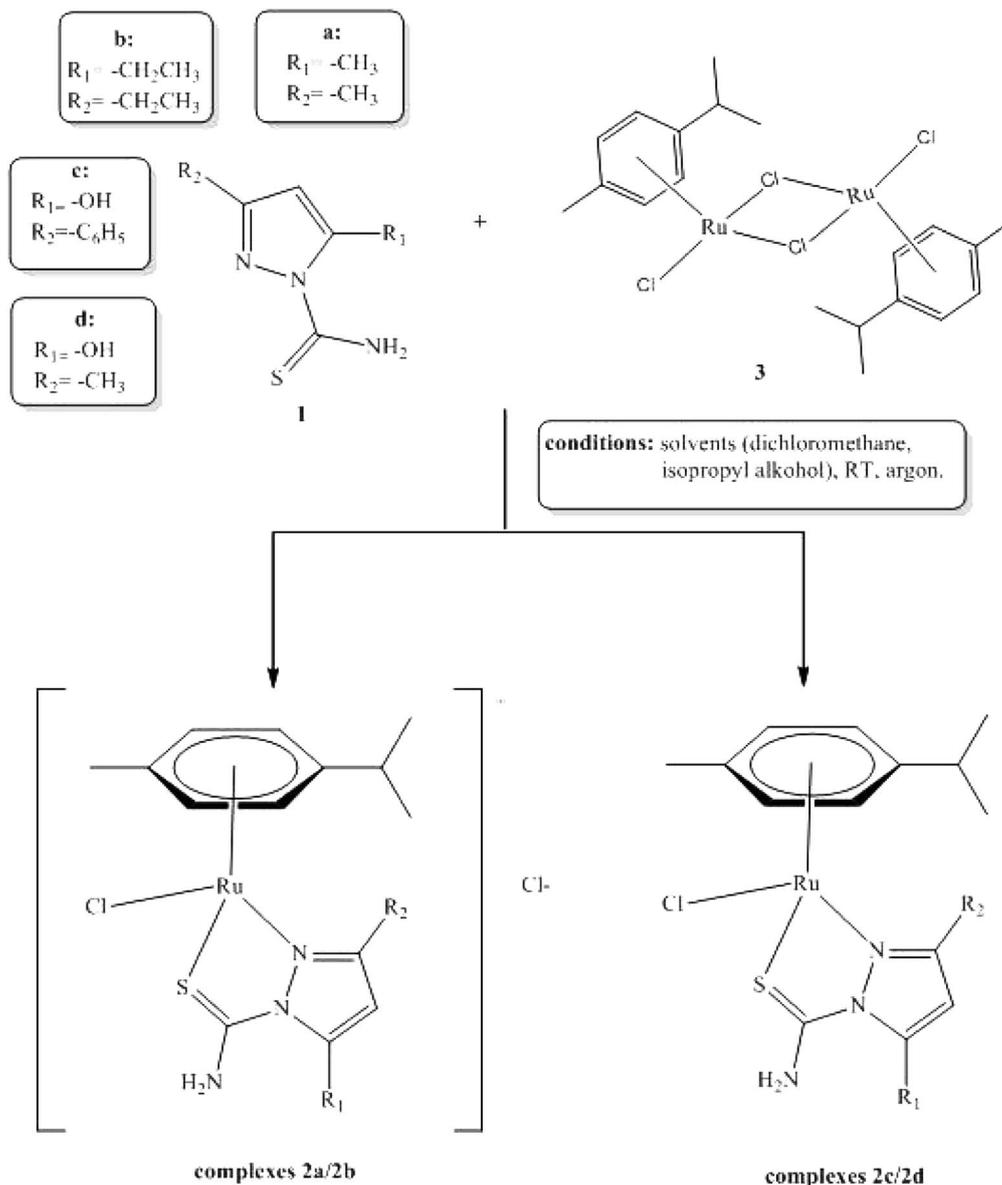
Scheme 3 General procedure of synthesis of arene–ruthenium(II) complexes **2a–2d**.

Table 2 ESI-MS date for the arene ruthenium(II) complexes **2a–2d**

| Complex	Type ions [XRuL]$^+$	Type ions [XRuLCl]$^+$	Sandwich ions	Ions in negative mode
2a	388.1(34%), 389.1(42%), 390.1(72%), 392.0(40%)	423.1(42%), 425(69%), 426.1(100%), 427.1(36%), 428.0(76%)	811.9(11%), 812.9(13%), 813.6(10%), 814.8(19%), 815.6(13%), 816.9(10%)	Not observed
2b	415.1(45%), 416.1(49%), 417.1(59%), 418.1(100%), 419.1(33%), 420(74%)	452.1(20%), 453.1(43%), 454.1(63%), 456.0(54%)		Not observed
2c	451.1(42%), 452.2(39%), 453.1(63%), 454.1(100%), 456.0(60%)	Not observed		486.4(29%), 487(64%), 488.3(100%), 489.3(35%), 490(64%)
2d	389.1(34%), 390.1(38%), 394.1(52%), 392.1(100%), 394.1(54%)	426.1(9%), 426.9(8%), 428.1(15%), 430.1(11%)	780.0(6%), 781.0(5%), 782.0(12%), 782.4(6%), 783.0(11%), 783.8(4%)	Not observed
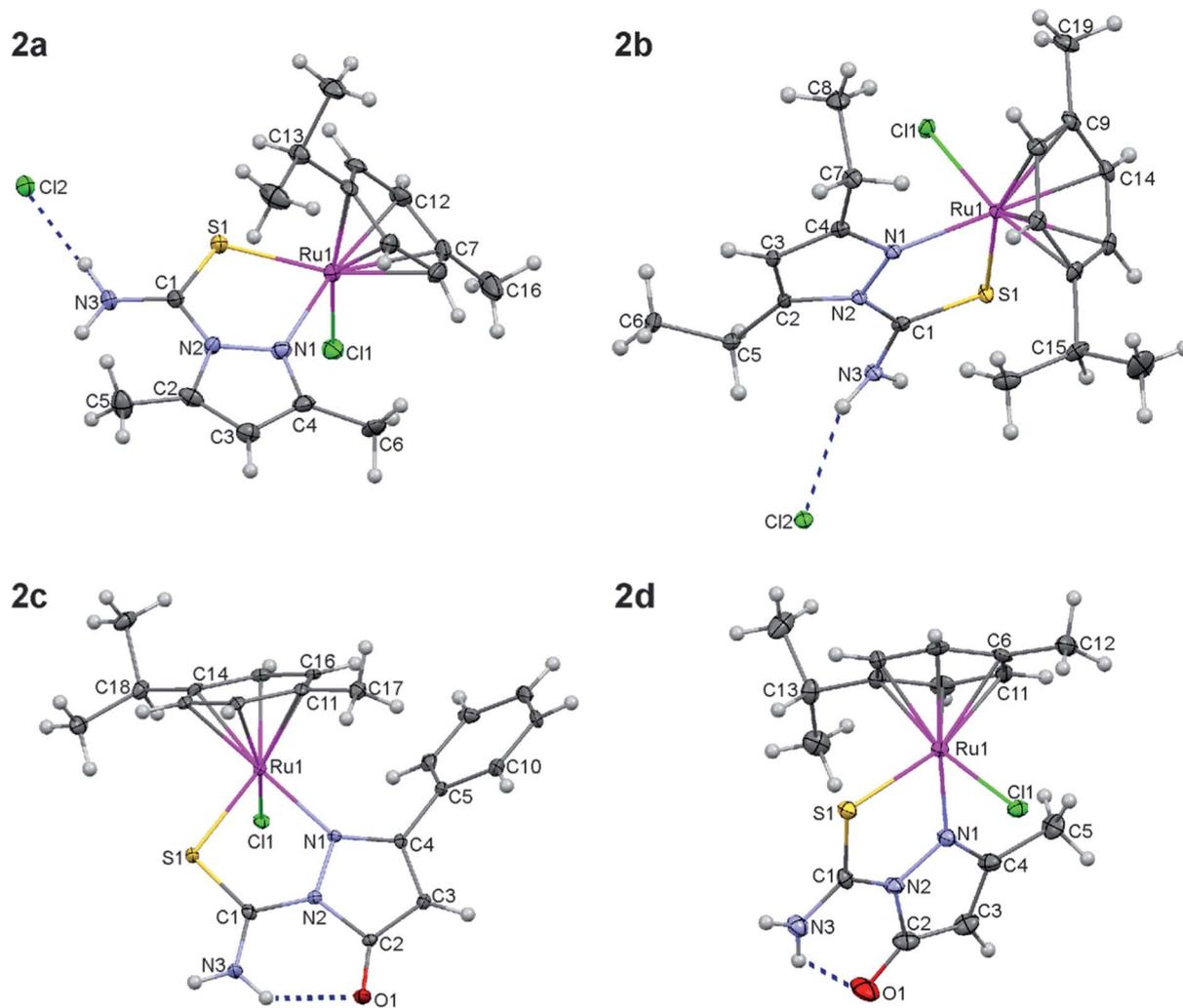
Fig. 1 Molecular structures of **2a–2d** with the labeling scheme. Thermal ellipsoids at 50% level. Hydrogen bonds indicated with dashed lines. Solvating molecules in **2a** (dichloromethane) and **2d** (water) not shown.

complex ions in **2a** and **2b** are accompanied by chloride counter ions. Interestingly, the changes in the molecular geometry, triggered by the change in the character of the heteroorganic ligand (neutral *vs.* anionic), are not conspicuous. They are rather visible within the ligands than in the ligand – metal interaction.

Carbon–oxygen bond in **2c** and **2d** is short – 1.250 Å – indicating the double bond character of the C=O group; in carbonyl compounds, it is approximately 1.21–1.23 Å, single C–O is usually around 1.43 Å. The carbonyl bond of the ligand in **2c** and **2d** is slightly elongated in comparison with the typical range but this may be explained by the hydrogen bonding interaction between O1 and the adjacent amino group. Crystal structures of **2c** and **2d** prove that binding to the metal ion forces the mesomeric structure II of the deprotonated ligands **1c** and **1d** as illustrated in Scheme 4.

Deprotonation of the hydroxyl ligands **2c** and **2d** influences C3–C4 within the pyrazole ring; the bond is shortened in comparison to the analogous bond in **2a** and **2b** because of

larger double bond character, whereas N1–N2 become slightly longer because of the electrostatic repulsion (see Table 3 and Scheme 3). However, the bonds to Ru remain almost the same for nearly all surrounding atoms in all complexes with the exception of Ru–Cl1 which is elongated by *ca.* 0.021 Å in the neutral **2c** and **2d**. It may be also noticed that Ru–CPC (see Table 1 for explanation) is slightly shortened in **2c/2d**.

The exchange of neutral ligands for anionic ones does not change the "stiff" piano-stool geometry typical for the Ru(II)–arene complexes *e.g.*;[26–30] the angles around Ru atom remain alike in all the studied compounds (Table 3). The overlays of the structures are presented in ESI as Fig. 3S.† As it was shown in Fig. 3S,† **2a** and **2d** adopt the most similar geometry; thus, it can be concluded that the mutual position of the ligands is mainly guided by the steric hindrance, exerted by the substituents and not by the charge on the ligand.

Pseudo-tetrahedral coordination of four different ligands makes all complexes chiral but three out of four compounds crystallize in centrosymmetric groups as racemic mixtures. Only

Table 3 Bond lengths [Å] and angles [°] for **2a–2d**

	2a	**2b**	**2c**	**2d**
Bond lengths [Å]				
Ru1–N1	2.101(8)	2.104(2)	2.109(4)	2.087(6)
Ru1-centroid of *p*-cymene (CPC)	1.704	1.691	1.683	1.688
Ru1–S1	2.357(3)	2.3260(7)	2.3635(12)	2.369(2)
Ru1–Cl1	2.411(3)	2.4144(7)	2.4393(11)	2.429(2)
S1–C1	1.693(10)	1.686(3)	1.688(4)	1.703(10)
N2–N1	1.385(10)	1.401(3)	1.410(5)	1.404(9)
N2–C1	1.401(12)	1.393(3)	1.368(5)	1.353(11)
N2–C2	1.416(12)	1.397(3)	1.438(5)	1.434(11)
N1–C4	1.333(13)	1.326(3)	1.346(5)	1.326(10)
C1–N3	1.309(12)	1.313(4)	1.312(6)	1.320(11)
C4–C3	1.419(14)	1.416(4)	1.395(6)	1.403(12)
C2–C3	1.351(14)	1.359(4)	1.406(6)	1.375(14)
C2–O1	—	—	1.250(5)	1.254(11)
Angles [°]				
N1–Ru1–CPC	132.44	135.14	134.08	132.16
N1–Ru1–S1	79.7(2)	80.93(6)	81.72(10)	80.9(2)
S1–Ru1–CPC	127.42	125.21	126.44	126.34
N1–Ru1–Cl1	84.2(2)	81.90(6)	84.55(10)	83.7(2)
Cl1–Ru1–CPC	127.43	128.84	126.46	128.22
S1–Ru1–Cl1	89.50(10)	89.14(8)	87.62(4)	89.64(8)

**2d** crystallized as one of two enantiomers in a chiral $P2_12_12_1$ space group.

The crystal packings and intermolecular interactions in solid **2a–2d** are presented in ESI (Fig. 4S–8S†). Except for **2d**, the complexes usually form hydrogen bonded dimers in the solid state. In the crystals of **2d**, additional molecule of water, inserted between the molecules of Ru(II) complex, creates more complicated pattern of hydrogen bonds leading to the formation of 1D chain that is aligned approximately along the *a*-axis. Parameters of intra- and intermolecular hydrogen bonds are collected in Table 1S of the ESI.†

3.4. Antimicrobial activity

Direct antimicrobial activity of arene–ruthenium(II) complexes with a carbothioamidopyrazole derivatives **2a–2d**, as well as the ligands alone **1a–1d** and dimer, was tested on representatives of pathogenic, opportunistic and commensal microorganisms, including staphylococci, enterococci, *Pseudomonas*, *Proteus* and *Candida*. The results of minimal inhibitory concentration (MIC)

and minimal bactericidal/fungicidal concentration (MBC/MFC) are presented in Table 4.

Antimicrobial effect of the compounds tested was observed against Gram-positive bacteria: *Staphylococcus aureus*, *Staphylococcus epidermidis* and *Enterococcus faecalis*, while all tested compounds had influence on Gram-negative bacteria (*Pseudomonas aeruginosa*, *Proteus vulgaris*) growth over the concentration range that was tested. The only exception was weak antimicrobial activity of **1b** and **2d** against *P. vulgaris* ATCC 8427 with MIC/MBC level of 1000 μg ml⁻¹. It has to be noted that antimicrobial effect was observed for arene–ruthenium(II) complexes, while dimer alone and most of the used ligands remained inactive. Even if selected ligand possessed antimicrobial activity against defined microbial strain, such as **1c** against *S. epidermidis* ATCC 12228 and *E. faecalis* ATCC 29212 (MIC at 62.5 μg ml⁻¹ and 500 μg ml⁻¹, respectively), the activity of corresponding complex **2c** in the same configurations was more than 2-fold and 16-fold, respectively, stronger (MIC < 31.2 μg ml⁻¹). Only compounds **2a** and **2b** were active against
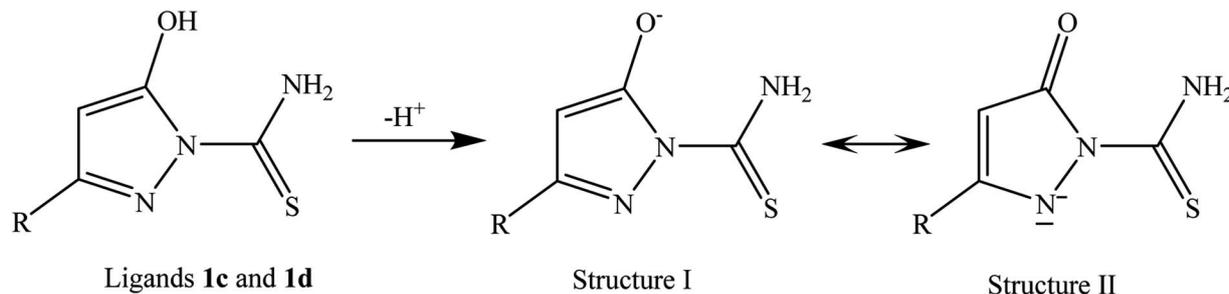
Scheme 4 Mesomeric structures of deprotonated ligands **1c** and **1d**.

Table 4 Antimicrobial activity of arene–ruthenium(II) complexes with carbothioamidopyrazole derivatives **2a–2d**, the ligands alone **1a–1d** and dimer. Minimal inhibitory concentrations (MIC) measured by broth microdilution assay. Minimal bactericidal/fungicidal (MBC/MFC) determined subsequently on the basis of microbial growth on solid media

Compound	MIC [μg ml^{-1}] MBC/MFC [μg ml^{-1}]					
	S. aureus ATCC 29213	S. epidermidis ATCC 12228	E. faecalis ATCC 29212	P. aeruginosa ATCC 25619	P. vulgaris ATCC 8427	C. albicans ATCC 10231
1a	>1000	>1000	>1000	>1000	>1000	>1000
	>1000	>1000	>1000	>1000	>1000	>1000
1b	1000	>1000	>1000	>1000	1000	1000
	>1000	>1000	>1000	>1000	1000	1000
1c	1000	62.5	500	>1000	>1000	>1000
	>1000	1000	>1000	>1000	>1000	>1000
1d	1000	250	250	>1000	>1000	>1000
	>1000	250	>1000	>1000	>1000	>1000
2a	125	62.5	62.5	>1000	>1000	250
	125	125	125	>1000	>1000	>1000
2b	62.5	31.2	62.5	>1000	>1000	250
	125	62.5	62.5	>1000	>1000	>1000
2c	31.2	<31.2	<31.2	>1000	>1000	>1000
	62.5	<31.2	<31.2	>1000	>1000	>1000
2d	500	500	500	>1000	1000	1000
	500	500	1000	>1000	1000	>1000
Dimer	>1000	>1000	>1000	>1000	>1000	1000
	>1000	>1000	>1000	>1000	>1000	>1000

Candida albicans with MIC at 250 μg ml^{-1}. However, both complexes indicated only fungistatic, but not fungicidal activity (MFC above the tested concentration range).

Initially, arene–ruthenium(II) complexes were not going to be used as antimicrobial agents. However, considering the fact that human microbiome plays an important role in preservation of healthy skin balance and mucous membrane barriers, as well as taking into account the etiology of many pathological changes (*e.g.* wound infections, cancer ulcerations), it is important to test antimicrobial activity of potential therapeutics. Epidemiological data indicate that wound infections frequently occur in patients with cancer, particularly with breast, head and neck cancers, as well as melanoma. The wound results from the tumor cells that infiltrate the skin and underlying tissues (malignant wounds) or is a consequence of complications of medical procedures (surgery, radiotherapy, chemotherapy).[33–35] Since patients with cancers are mostly affected by opportunistic infections with a predominance of staphylococci as their etiological agents, the results in which we demonstrated biostatic and biocidal effect of tested complexes (mainly **2a–2c**) against Gram-positive bacteria, such as *S. aureus*, *S. epidermidis*, and *E. faecalis*, seem to be favorable. Potential local application of tested arene–ruthenium(II)complexes on the skin could simultaneously reduce the development of melanoma cells and protect against wounds infections. Nevertheless, the range of antimicrobial activity of such preparations strongly depends on their structure and composition. For example, we did not observe biocidal activity of arene–ruthenium(II)complexes against Gram-negative bacteria and *Candida* yeast, while Kulkarni *et al.*[36] demonstrated good activity of the pyrazole-based copper complexes with

thiosemicarbazide arms against *E. coli* and *P. aeruginosa*, comparable with gentamycin activity, when they used 500 μg of the compounds in the disc-diffusion method. At the same time, other transition metal *e.g.* Co(II), Ni(II), and Zn(II) complexes did not show such significant antimicrobial activity.[37] Similar discrepancies in the antimicrobial activity were observed by Mandal *et al.*[37] who described a strong biostatic effect of cadmium and mercury complexes of 5-methyl pyrazole-3yl-*N*-(20-methylthiophenyl) methyleneimine, (MPzOATA) ligand, against some Gram-positive and Gram-negative bacteria, while nickel complexes with the same ligands ([Ni(MPzOATA)$_2$](-Cl)(PF$_6$); [Ni(MPzOATA)$_2$](ClO$_4$)$_2$CH$_3$CN; [Ni(MPzOATA)$_2$](BF$_4$)$_2$-H$_2$O) did not express such activity. Interestingly, the MICs of cadmium and mercury complexes against *S. aureus* reached similar values (35 μg ml^{-1} and 20 μg ml^{-1}, respectively) as our **2b** and **2c** ruthenium complexes.[38] Therefore, we postulate that every single new anticancer drug should be assessed for its antimicrobial effect specific test microorganisms, selected on the basis of its potential site of application and formulation.

3.5. Cytotoxic activity

To test cytotoxicity of arene–ruthenium(II) complexes with carbothioamidopyrazole derivatives **2a–2d**, as well as the ligands alone **1a–1d** and dimer against regular eukaryotic cells, human foreskin fibroblasts HFF-1 (ATCC-SCRC-1041) were chosen. The influence of tested compounds on the cell viability is shown in Fig. 2.

Neither ligands nor dimer alone were cytotoxic against human fibroblasts over the tested concentration range. IC$_{50}$ values were as high as 1220.5; 1740.2; 1001.1; 1384.0 μM for **1a–1d**, respectively, and 1211.2 μM for dimer. Most of arene–
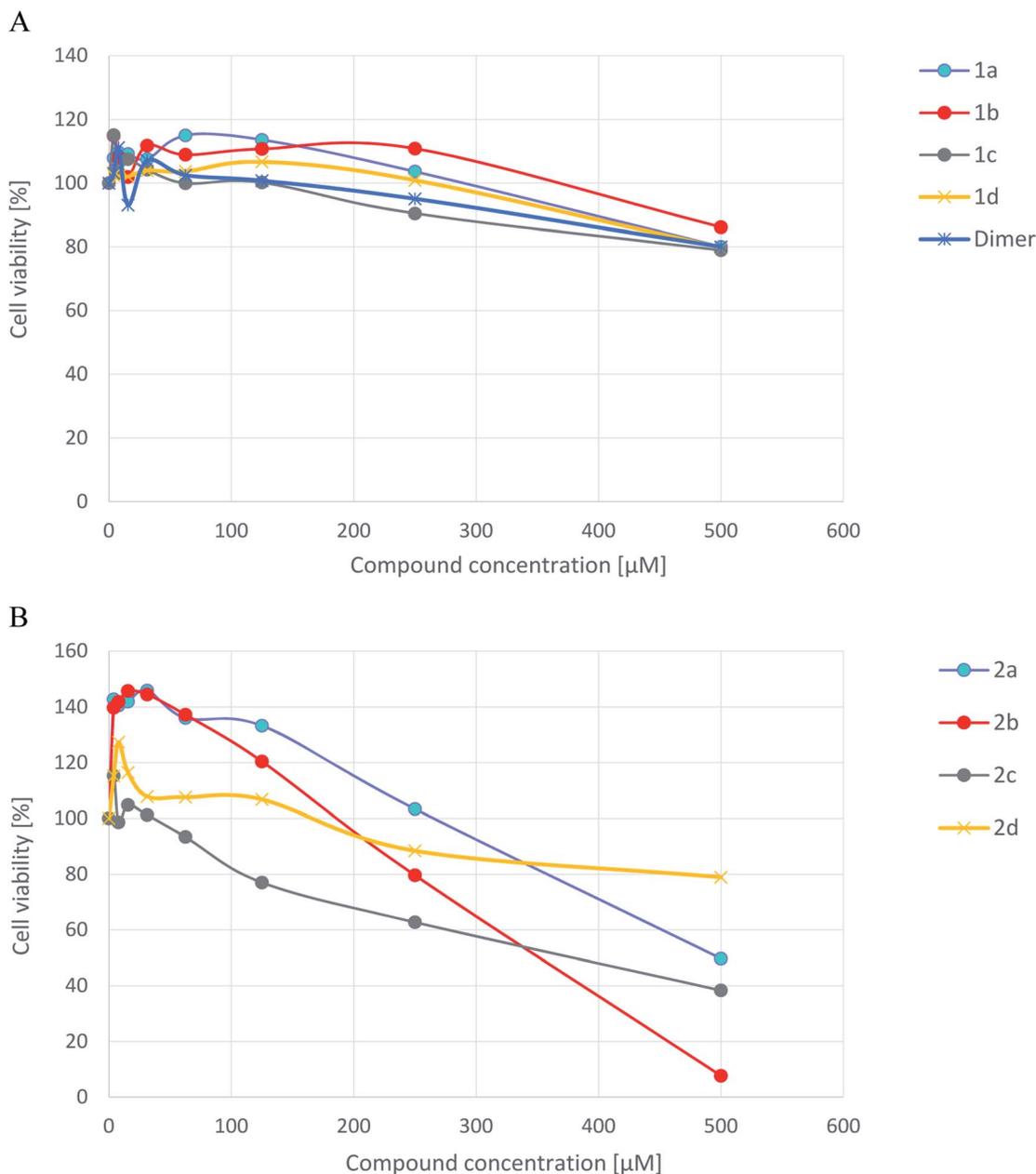
Fig. 2 Cytotoxicity of ligands **1a–1d** and dimer [A], and arene–ruthenium(ɪɪ) complexes **2a–2d** [B] for human foreskin fibroblasts line HFF-1 measured by the MTT method.

ruthenium(ɪɪ) complexes with pyrazole derivatives indicated cytotoxicity against tested cell lines. The strongest cytotoxicity showed complexes **2b** and **2c** with IC_{50} values 358.3 µM and 381.4 µM respectively. Slightly weaker cytotoxic effect indicated compound **2a** with IC_{50} value 545.1 µM. The viability of HFF-1 cells did not drop below 80% in the presence of compound **2d** (no cytotoxic effect), for which IC_{50} value was 850.5 µM. Interestingly, the complexes **2a** and **2b** used at low concentrations (3.9–31.2 µM) seems to stimulate human fibroblast divisions (metabolic activity of those cells was about 39–45% higher than untreated control cells). However, the possible mitogenic activity of **2a** and **2b** arene–ruthenium(ɪɪ) complexes requires confirmation in the future studies.

3.6. Anticancer activity of novel ruthenium complexes

The *in vitro* anticancer activity was tested for all obtained arene–ruthenium(ɪɪ) compounds **2a–2d** and their ligands **1a–1d** against HL-60 (leukemia promyelocytic), NALM-6 (leukemia lymphoblastic) and WM-115 (human melanoma) cell lines. Also, dichloro(*p*-cymene)ruthenium(ɪɪ) dimer was tested against the above cell lines. Cisplatin and carboplatin were used as a ref. 31. The colorimetric MTT assay was used to determine the influence of broad range of compounds concentrations (from 10^{-7} to 10^{-5} M) on cells lines (exposure time was 48 h). Obtained results, expressed as IC_{50} values for all tested compounds, are presented in Table 5.

Table 5 Results of anticancer activity of newly synthesized compounds

Compounds	Cell culture IC$_{50}$^{a} [μM]		
	HL-60	NALM-6	WM-115
1a	583.9 ± 84.3	569.3 ± 21.9	>1000
1b	506.37 ± 47.08	468.52 ± 44.36	481.29 ± 39.43
1c	618.0 ± 32.0	152.3 ± 26.7	751.5 ± 118.1
1d	778.8 ± 125.3	614.7 ± 60.9	90.91 ± 10.2
2a	88.86 ± 6.06	51.55 ± 5.71	60.24 ± 6.30
2b	80.83 ± 3.9	40.03 ± 5.59	54.88 ± 5.94
2c	86.51 ± 8.02	11.71 ± 1.62	26.66 ± 3.28
2d	594.0 ± 52.0	491.4 ± 31.0	7.99 ± 0.87
Dimer	400.86 ± 46.22	373.89 ± 40.78	>1000
Cisplatin^b	0.8 ± 0.1	0.7 ± 0.3	18.2 ± 4.3
Carboplatin^b	4.3 ± 1.3	0.7 ± 0.2	422.2 ± 50.2

^{a} IC$_{50}$ values [μM] were calculated at concentration of a tested compound required to reduce the fraction of surviving cell to 50% of that observed in comparison to the control probe, non treated cell. Mean values are presented of parameter IC$_{50}$ ± SD from 4 experiments. ^{b} The values for referential compounds can be found in literature.[23]

The highest antitumor activity was observed for complex **2d** against WM-115 cell line (IC$_{50}$ = 7.99 ± 0.87 μM), while complex **2c** was the most active against NALM-6 cell line (IC$_{50}$ = 11.71 ± 1.62 μM). It went out that compound **2d** is more cytotoxic than cisplatin and carboplatin. IC$_{50}$ values for complexes **2a–2c** were similar to each other against HL-60, NALM-6 and WM-115 cell lines and at the same time lower than for ligands. Complex **2d** was inactive against acute leukemia (HL-60) as well as lymphoblastic (NALM-6) cell lines. All ligands **1a–1d** and dichloro(p-cymene)ruthenium(II) dimer were inactive against all the tested cell lines: HL-60, NALM-6 and WM-115.

IC$_{50}$ values for complexes **2a–2c** against all tested cancer cell lines (HL-60, NALM-6, WM-115) were achieved at the concentration range from 11.7 to 88.9 μM, while against normal fibroblasts HFF-1 the same effect was observed at a concentration above 358 μM. The anticancer activity of **2d** complex was strongly dependent on the used cell line. The best results were observed against melanoma cell line WM-115 with the activity above 2-fold stronger than cisplatin (7.9 μM versus 18.2 μM of IC$_{50}$ values, respectively). Based on IC$_{50}$ values arene–ruthenium(II) complexes with a pyrazole might be good alternative to cisplatin. A similar cytotoxic effect of **2d** against HL-60 and NALM-6 was achieved only for concentration above 491 μM. The application of complex **2d** as anticancer agent seems to be safe because as it was already mentioned before 50% cytotoxicity against HFF-1 cells was obtained at the concentration 850.5 μM.

3.7. Cleavage of pUC57 DNA

The cleavage of plasmid pUC57 DNA by tested compounds was tested with gel electrophoresis.

The supercoiled form of DNA (Form I) that occurs naturally, when nicked, gives an open circular relaxed form (Form

II) and further cleaves to a linear form (Form III). During electrophoresis, Form I shows the fastest migration compared to Forms II and III. Form II migrates slowly prior to its relaxed structure, while Form III migrates between the positions of Forms I and II.[32] Pure DNA diluted in the mixture of DMSO (the same amount as for tested compounds) + TrisHCl/NaCl buffer without treatment with tested compound was used as control.

Lanes 1–17 (Fig. 3) represent DNA incubated with increasing amounts of the complexes, with concentrations of 50, 100 and 150 μM, respectively (results of the usage of 150 μM of compound are presented only for compound **2d** and **2a**). In most cases, complex concentration above 150 μM produced DNA sedimentation (except dimer compound that caused DNA sedimentation even in concentration 50 μM).

The results indicated that chosen ruthenium(II) complexes **2b, 2d** can play a similar role as nucleases by cleavage the DNA Form I into Form II and Form III. It seems that both complexes are able to cut the DNA strand at two positions. The complexes cause an increase in the band intensity of Form III, while the intensity of Form I progressively decreased and these effects are definitely dependent on the concentration of the tested compound.

Compound **2a** and **2c** have no influence on the supercoiled plasmid DNA in any of tested concentrations.

All tested ligands **1a–1d** as well as dimer **3** have no effect on the DNA strands, which means that the effect caused by compounds **2b, 2d** is a result of their complex structures, not the activity of the ligands alone. However, it has to be noticed that only small concentrations of the dimer were used to the studies as it caused strong sedimentation of the DNA in higher concentrations.

The cytotoxicity of ruthenium complexes against cancer cell lines might be related to their ability to interactions with DNA.[38,39] Many metal complexes can change the structure and stability of DNA by hydrogen bonding and π stacking between its strands.[40] It has been well documented that transition–metal complexes are not only able to interact with DNA but also to damage its structure as well as other cellular structures. This might be a promising strategy for anticancer drug design.[41] It has been proved that DNA is the main biological target of cisplatin – the successful anticancer drug.[42] Ruthenium(II)–arene complexes similarly to cisplatin are less reactive at high chloride concentrations (e.g. in blood plasma), while at low chloride concentrations inside a cell, they are activated by aquation and then are able to interact with DNA and proteins.[43,44]

The cytotoxic effect of compounds **2b, 2d** might be related to their ability to cleave the DNA as they cut the supercoiled DNA in two positions leading to the linear form of the DNA. It was also proved that the influence of complexes **2b, 2d** on the DNA structure is associated with their own activity as ligands **1a, 1b, 1d** did not affect the DNA. However it has to be noted, that while although DNA binding could be the mechanism of action, other factors e.g. cell uptake will have an influence on the cytotoxicity and can depend on the nature of the compound.

A   **B**
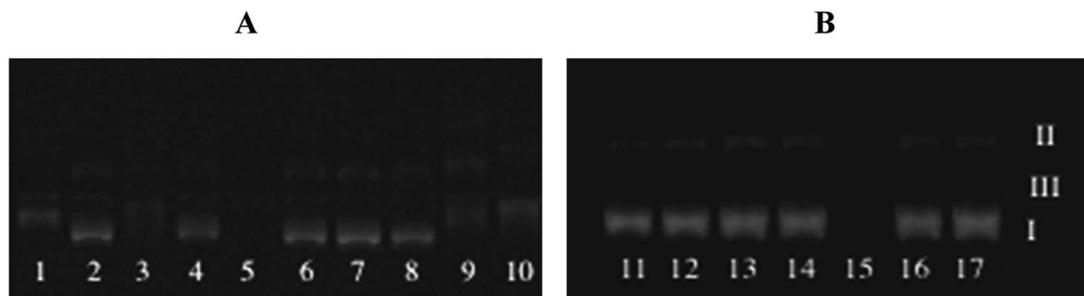
Fig. 3   Gel electrophoresis diagrams showing the cleavage of supercoiled pUC57 DNA (A) (1) DNA + 100 μM compound **2a**, (2) DNA + 50 μM compound **2a**, (3) DNA + 100 μM compound **2b**, (4) DNA + 50 μM compound **2b**, (5) DNA + 150 μM compound **2b**, (6) DNA + 100 μM compound (**2c**), (7) DNA + 50 μM compound **2c**, (8) DNA + 50 μM compound **2d**, (9) DNA + 100 μM compound **2d**, (10) DNA + 150 μM compound **2d**. (B) (11) DNA + 100 μM compound **2a**, (12) DNA + 100 μM compound **1b**, (13) DNA + 100 μM compound **1c**, (14) DNA + 100 μM compound **1d**, (15) DNA + 50 μM dimer, (16) DNA + 20 sμM dimer.

3.8. DFT calculations

The results of DFT calculations confirm the correctness of the measured structures and diamagnetic character of Ru(II) in the studied complexes. The basic pseudotetrahedral structures were preserved during the geometry optimizations (energy minimization procedure) as shown in Fig. 6S.† Important bond lengths and bond angles of coordinated ligands in the X-ray experimental and calculated structures are compared in Table 2S.† Major shifts during the optimization procedure were connected with the positions of chloride anions, which were

deprived of the nearest neighbors. Though the molecule of water was not included in the calculated structure of **2d**, the geometry of this complex molecule remained approximately constant during the optimization procedure. Calculations confirm the effects observed in the experimental structures for example they show the strengthening of Ru-*p*-cymene centroid bonds within the molecular complexes in comparison to cationic ones.

The electronic structures are obviously different for the pair of cationic complexes **2a** and **2b** and molecular **2c** and **2d**. Orbitals HOMO of the cationic species are built from localized p
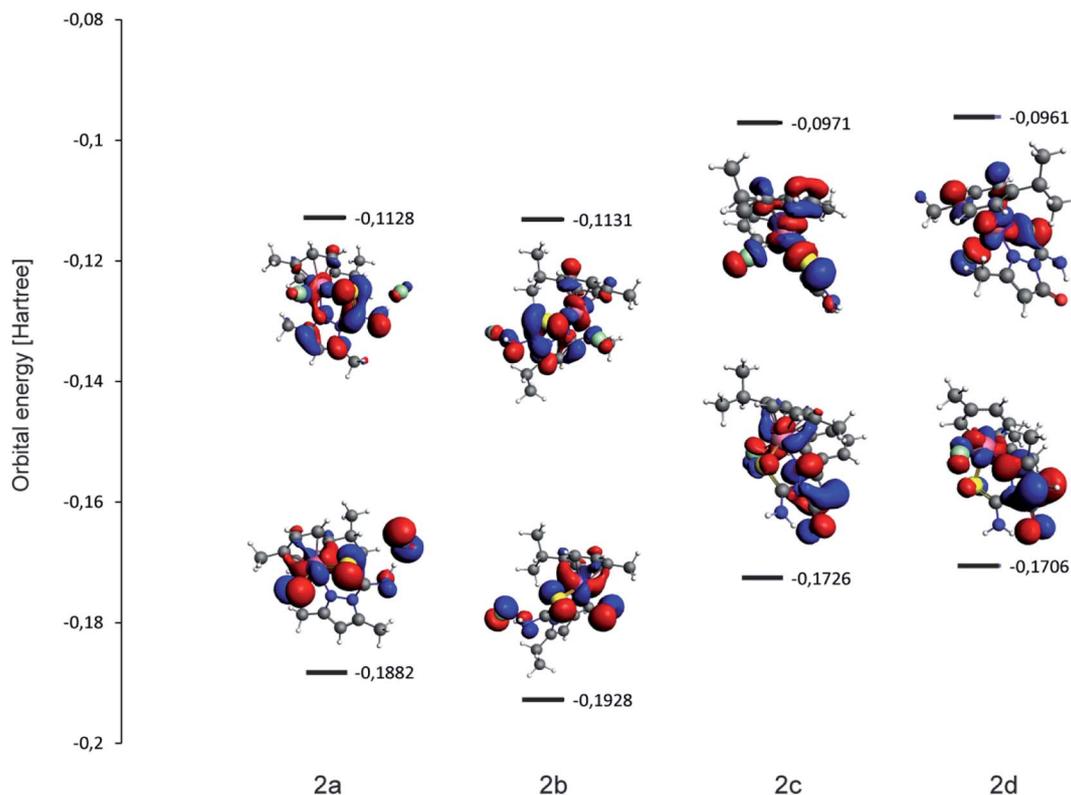
Fig. 4   The calculated (DFT BP86-D/TZP) energies and shapes of frontier orbitals in the studied complexes **2a**–**2d**. The HOMO−LUMO gaps are: **2a** − 0.0754 hartree (2.052 eV); **2b** − 0.0797 hartree (2.169 eV); **2c** − 0.0755 hartree (2.054 eV); **2d** − 0.0745 hartree (2.027 eV).
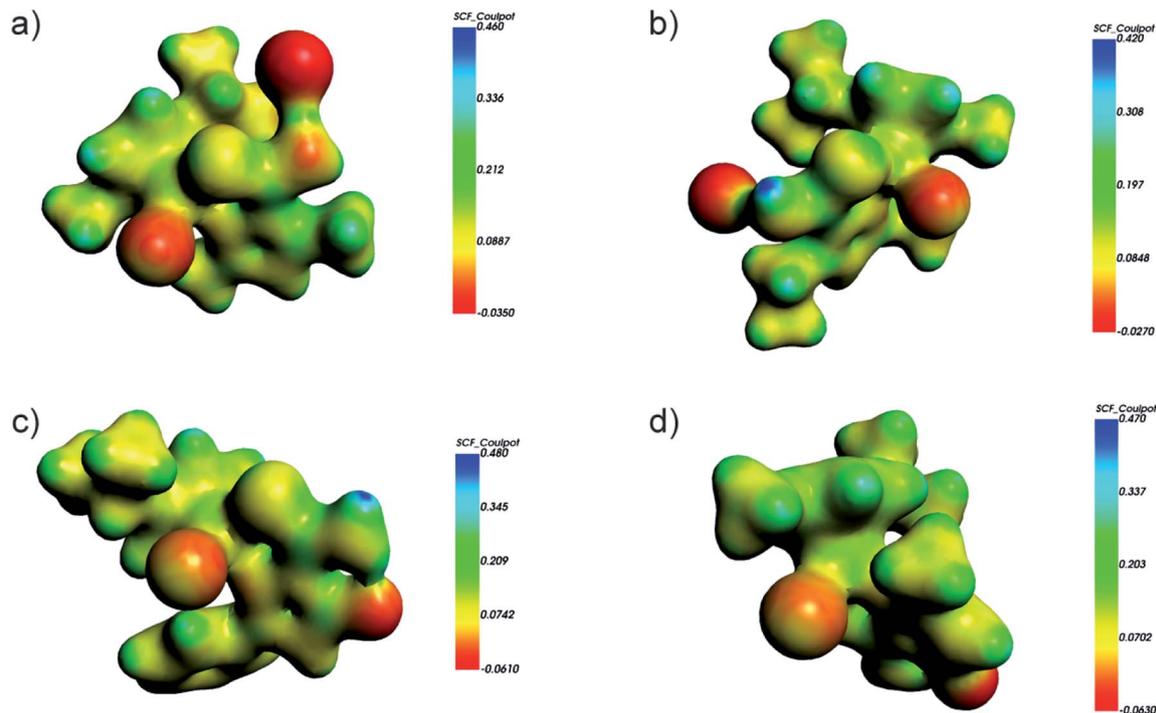
Fig. 5 The calculated (DFT BP86-D/TZP) electrostatic potential mapped at the isodensity surface 0.03 for: (a) **2a**; (b) **2b**; (c) **2c**; (d) **2d**.

orbitals of sulfur and nitrogen atoms of N,S-organic ligands, whereas the corresponding HOMO orbitals of molecular complexes have a large contribution of delocalized π orbitals of pyrazole ligands (Fig. 4).

Molecular electrostatic potential (MEP) maps of **2a–2d** illustrated in Fig. 5 show the distribution of charge on the isodensity surface 0.03. Though the relatively large differences between the minimum and maximum values of MEP are expected for the ionic complexes **2a** and **2b**, they are even larger for molecular species **2c** and **2d**, which was not obvious before the analysis. The minimum values of MEP for **2c** and **2d** are located at the oxygen O1 atom of the pyrazole ligand and the lowest value of -0.063 eV considering all the studied complexes

is reached for **2d**. Interestingly, the crystal structure of **2d** features a molecule of water hydrogen bonded to O1, which is a nice experimental proof of the relatively large negative MEP value connected with O1 within this complex.

The charge distribution within the complexes may be further described with the partial charges and dipole moments collected in Table 6. Despite the different character of the complex species the partial charge of the Ru, which is often connected with the cytotoxicity of ruthenium complexes [45] remains within relatively narrow range. The major difference is noticed for **2a** and here the partial positive charge of Ru is lowest, which is in agreement with the lowest cytotoxicity in most studied concentrations as discussed in the previous

Table 6 Calculated partial charges of selected atoms in complexes **2a–2d** and their dipole moments

| Atom | Complex | | | | | | | |
| | 2a | | 2b | | 2c | | 2d | |
	Mulliken	Hirshfeld	Mulliken	Hirshfeld	Mulliken	Hirshfeld	Mulliken	Hirshfeld
Ru1	+0.381	+0.276	+0.420	+0.284	+0.449	+0.286	+0.461	+0.284
Cl1	−0.400	−0.292	−0.386	−0.278	−0.398	−0.274	−0.397	−0.300
Cl2	−0.520	−0.389	−0.528	−0.383	—	—		
S1	+0.041	−0.005	−0.036	−0.043	−0.069	−0.074	−0.076	−0.068
O1	—	—			−0.618	−0.273	−0.615	−0.271
N1	−0.304	−0.059	−0.326	−0.062	−0.339	−0.091	−0.345	−0.096
N2	+0.084	+0.032	−0.076	+0.040	−0.089	+0.008	−0.116	+0.007
N3	−0.099	−0.143	−0.139	−0.143	+0.052	−0.134	+0.010	−0.138
Dipole moments [D]								
	9.945		7.418		6.929		7.004	

chapters. The large negative partial charge is connected with O1 and according to the charges arising from the Mulliken population analysis it is even higher than negative charge ascribed to the chloride anion Cl2. The dipole moments are comparable for **2c** and **2d**. The largest value of the dipole moment of **2a** seems to be more connected with the spatial arrangement of atoms than the charge separation.

Another calculated feature that may be compared with the cytotoxicity results is HOMO–LUMO gap illustrated in Fig. 4 (together with the shape of frontier orbitals). Low energy separation of frontier orbitals is correlated with complex reactivity and geometrical flexibility (the ease of excitation). As listed in Fig. 4 caption there are no major differences between the studied complexes, however complex **2b** features the largest HOMO–LUMO gap of 2.169 eV and in **2d** the gap is smallest (2.027 eV) thus the value is not related to the ionic/molecular character of the complex.

4. Conclusions

In response to the demand for effective anticancer drugs, the new arene–ruthenium(II) complexes were synthesized. All compounds were obtained with high yields. X-ray experiment indicated that all complexes have nitrogen–sulfur coordination create piano stool complexes. Electrospray ionization mass spectrometry confirmed complexes structure **2a–2d** in solid and solution. An analysis of ESI-MS spectra shows that all used compounds are stable in solutions and it is difficult to break ruthenium–sulfur coordination bonds or permanent nitrogen in tandem reactions. Coordination bonds in all complexes **2a–2d** are stable and not fragmented, whereas other bonds decompose in these molecules. It was demonstrated, that the various structure of these complexes (presence of carbonyl, hydroxyl, phenyl groups in pyrazole ring) influenced their biological activity, including anticancer effect. It has to be noted that compound **2d** showed higher cytotoxicity against melanoma cell line WM-115 than cisplatin. The compound **2c** demonstrated good activity against lymphoblastic cell line NALM-6. Although the new arene–ruthenium(II) complexes indicated moderated cytotoxicity also against normal eukaryotic cells, as well (see the effect against human fibroblasts line HFF-1) the application of tested complexes, based on IC$_{50}$ values (stronger cytotoxic effect against cancer than regular cells), seems to be still safe. The cytotoxic effect of compounds **2b**, **2d** might be a result of their ability to cleave the DNA. Assuming that new preparations will appear to have a more universal effect, a huge part of this research was focused not only on their anticancer, but also on antimicrobial activity. A potential application of tested complexes on skin or mucous membranes can affect opportunistic activity of natural microbiota and well as pathogens, which often cause wound infections in cancer patients. As new arene–ruthenium(II) compounds indicated biostatic and biocidal activity against Gram-positive bacteria, including *S. aureus*, *S. epidermidis* and *E. faecalis*, they could not only inhibit proliferation of cancer cells, but also protect the patients against malignant wound infections. Nevertheless,

further studies, including *in vivo* tests, are necessary in this regard.

The DFT analysis proved that there is no simple correlation between the ionic/molecular character of the complex and its features such as partial charges, dipole moments or HOMO–LUMO separations.

Conflicts of interest

The authors declare no conflict of interests.

Acknowledgements

References

1 A. K. Singh, D. S. Pandey, Q. Xu and P. Braunstein, *Coord. Chem. Rev.*, 2014, **270–271**, 31–56.

2 S. B. Fricker, *Dalton Trans.*, 2007, **43**, 4903–4917.

3 Z. Ude, I. Romero-Canelón, B. Twamley, D. Fitzgerald Hughes, P. J. Sadler and C. J. Marmion, *J. Inorg. Biochem.*, 2016, **160**, 210–217.

4 T. S. Morais, T. J. L. Silva, F. Marques, M. P. Robalo, F. Avecilla, P. J. A. Madeira, P. J. G. Mendes, I. Santos and M. H. Garcia, *J. Inorg. Biochem.*, 2012, **114**, 65–74.

5 A. Weiss, R. H. Berndsen, M. Dubois, C. Müller, R. Schibli, A. W. Griffioen, P. J. Dyson and P. Nowak-Sliwinska, *Chem. Sci.*, 2014, **5**, 4742–4748.

6 A. Srishailam, Y. P. Kumar, N. M. D. Gabra, P. V. Reddy, N. Deepika, N. Veerababu and S. Satyanarayana, *J. Fluoresc.*, 2013, **23**, 897–908.

7 G. Süss-Fink, *Dalton Trans.*, 2010, **39**, 1673–1688.

8 F. V. Rocha, C. V. Barra, A. V. G. Netto, A. E. Mauro, I. Z. Carlos, R. C. G. Frem, S. R. Ananias, M. B. Quilles, A. Stevanato and M. C. da Rocha, *Eur. J. Med. Chem.*, 2010, **45**, 1698–1702.

9 F. Wang, J. Xu, K. Wu, S. K. Weidt, C. L. MacKay, P. R. R. Langridge-Smith and P. J. Sadler, *Dalton Trans.*, 2013, **42**, 3188–3195.

10 G. S. Smith and B. Therrien, *Dalton Trans.*, 2011, **40**, 10793–10800.

11 S. Karabasannavar, P. Allolli, I. N. Shaikh and B. M. Kalshetty, *Indian J. Pharm. Educ.*, 2017, **51**, 490–501.

12 Z. K. Jaćimović, M. Kosović, S. B. Novaković, G. Giester and A. Radović, *J. Serb. Chem. Soc.*, 2015, **80**, 867–875.

13 A. Ansari, A. Ali, M. Asif and S. Shamsuzzaman, *New J. Chem.*, 2017, **41**, 16–41.

14 A. D. Kumar, S. Bharath, R. N. Dharmappa, S. Naveen, N. K. Lokanath and K. A. Kumar, *Res. Chem. Intermed.*, 2018, **44**, 5635–5652.

15 K. Karrouchi, S. Radi, Y. Ramli, J. Taoufik, Y. N. Mabkhot, F. A. Al-aizari and M. Ansar, *Molecules*, 2018, **23**, 1–86.

16 Y.-J. Cui, L.-Q. Tang, Ch-M. Zhang and Z.-P. Liu, *Molecules*, 2018, **23**, 1–9.

17 E. Budzisz, U. Krajewska, M. Różalski, A. Szuławska, M. Czyż and B. Nawrot, *Eur. J. Pharmacol.*, 2004, **502**, 59–65.

18 E. Budzisz, M. Malecka, I.-P. Lorenz, P. Mayer, R. Kwiecień, P. Paneth, U. Krajewska and M. Rozalski, *Inorg. Chem.*, 2006, **45**, 9688–9695.

19 M. Sobiesiak, I.-P. Lorenz, P. Mayer, M. Wozniczka, A. Kufelnicki, U. Krajewska, M. Rozalski and E. Budzisz, *Eur. J. Med. Chem.*, 2011, **46**, 5917–5926.

20 M. Grazul, E. Besic-Gyenge, C. Maake, M. Ciolkowski, M. Czyz, R. K. O. Sigel and E. Budzisz, *J. Inorg. Biochem.*, 2014, **135**, 68–76.

21 E. Namiecinska, M. Sobiesiak, M. Malecka, P. Guga, B. Rozalska and E. Budzisz, *Curr. Med. Chem.*, 2019, **26**, 664–693.

22 I. Radosavljević Evans, J. A. K. Howard, L. E. M. Howard, J. S. O. Evans, Z. K. Jacimović, V. S. Jevtović and V. M. Lovac, *Inorg. Chim. Acta*, 2004, **357**, 4528–4536.

23 M. Sobiesiak, T. Muzioł, M. Rozalski, U. Krajewska and E. Budzisz, *New J. Chem.*, 2014, **38**, 5349–5361.

24 M. Sobiesiak, M. Cieślak, K. Królewska, J. Kaźmierczak-Barańska, B. Pasternak and E. Budzisz, *New J. Chem.*, 2016, **40**, 9761–9767.

25 P. Pelagatti, M. Carcelli, F. Calbiani, C. Cassi, L. Elviri, C. Pelizzi, U. Rizzotti and D. Rogolino, *Organometallics*, 2005, **24**, 5836–5844.

26 J. Grau, V. Noe, C. Ciudad, M. J. Prieto, M. Font-Bardia, T. Calvet and V. Moreno, *J. Inorg. Biochem.*, 2012, **109**, 72–81.

27 A. A. Nazarov, C. G. Hartinger and P. J. Dyson, *J. Organomet. Chem.*, 2014, **751**, 251–260.

28 P. Kumar, R. K. Gupta and D. S. Pandey, *Chem. Soc. Rev.*, 2014, **43**, 707–733.

29 P. Rogala, A. Jabłońska-Wawrzycka, K. Kazimierczuk, A. Borek, A. Błażejczyk, J. Wietrzyk and B. Barszcz, *J. Mol. Struct.*, 2016, **1126**, 74–82.

30 J. M. Gichumbi, H. B. Friedrich and B. Omondi, *J. Organomet. Chem.*, 2016, **808**, 87–96.

31 E. Budzisz, U. Krajewska and M. Rozalski, *Pol. J. Pharmacol.*, 2004, **56**, 473–478.

32 R. R. Sinden, *DNA Structure and Function*, Academic Press Limited, London, 1994, pp. 131–133.

33 I. Fromantin, S. Watson, A. Baffie, A. Rivat, M. C. Falcou, I. Kriegel de Rycke and Y. Ingenior, *Ostomy/Wound Manag.*, 2014, **60**, 38–48.

34 W. G. Payne, D. K. Naidu, C. K. Wheeler, D. Barkoe, M. Mentis, R. E. Salas, D. J. Ir. Smith and M. C. Robson, *Eplasty*, 2008, **8**, e9.

35 K. Rolston, L. Nesher and J. T. Tarrand, *Infect. Dis. Ther.*, 2014, **3**, 245–256.

36 N. V. Kulkarni, A. Kamath, S. Budagumpi and V. K Revankar, *J. Mol. Struct.*, 2011, **1006**, 580–588.

37 S. Mandal, M. Mondal, J. K. Biswas, D. B Cordes, A. M. Z. Slawin, R. J. Butcher, M. Saha and N. Ch. Saha, *J. Mol. Struct.*, 2018, **1152**, 189–198.

38 C. X. Zhang and S. J. Lippard, *Curr. Opin. Chem. Biol.*, 2003, **7**, 481–489.

39 L. R. Ferguson and W. A. Denny, *Mutat. Res., Fundam. Mol. Mech. Mutagen.*, 2007, **623**, 14–23.

40 J. R. Aldrich-Wright, S. R. Vagg and P. A. Williams, *Coord. Chem. Rev.*, 1997, **166**, 361–389.

41 Y. Jung and S. J. Lippard, *Chem. Rev.*, 2007, **107**, 1387–1407.

42 K. Gkionis, J. A. Platts and J. Grant Hill, *Inorg. Chem.*, 2008, **47**, 3893–3902.

43 F. Wang, J. Bella, J. A. Parkinson and P. J. Sadler, *J. Biol. Inorg. Chem.*, 2005, **10**, 147–155.

44 F. Wang, H. Chen, S. Parsons, I. D. H. Oswald, J. E. Davidson and P. J. Sadler, *Chem. - Eur. J.*, 2003, **9**, 5810–5820.

45 Z. Sochorová Vokáčová, I. Turel and J. V. Burda, *J. Mol. Model.*, 2018, **24**, 98.

46 STOE and C. GmbH, *X-area - software package for collecting single-crystal data on STOE area-detector diffractometers, for image processing, scaling reflection intensities and for outlier rejection*, Darmstadt, Germany, 2015.

47 G. M. Sheldrick, *Acta Crystallogr., Sect. C: Cryst. Struct. Commun.*, 2015, **71**, 3–8.

48 O. V. Dolomanov, L. J. Bourhis, R. J. Gildea, J. A. K. Howard and H. Puschmann, *Appl. Crystallogr.*, 2009, **42**, 339–341.

49 L. J. Farrugia, *J. Appl. Crystallogr.*, 2012, **45**, 849–854.

50 C. F. Macrae, I. J. Bruno, J. A. Chisholm, P. R. Edgington, P. McCabe, E. Pidcock, L. Rodriguez-Monge, R. Taylor, J. van de Streek and P. A. Wood, *J. Appl. Crystallogr.*, 2008, **41**, 466–470.

51 European Committee on Antimicrobial Susceptibility Testing – EUCAST, http://www.eucast.org, 2012.

52 G. te Velde, F. M. Bickelhaupt, E. J. Baerends, C. Fonseca Guerra, S. J. A. van Gisbergen, J. G. Snijders and T. Ziegler, *J. Comput. Chem.*, 2001, **22**, 931–967.

53 C. Fonseca Guerra, J. G. Snijders, G. te Velde and E. J. Baerends, *Theor. Chem. Acc.*, 1998, **99**, 391–403.

54 ADF2018, SCM, *Theoretical Chemistry*, Vrije Universiteit, Amsterdam, The Netherlands, 2018, http://www.scm.com.

55 D. Becke, *Phys. Rev. A*, 1988, **38**, 3098–3100.

56 C. Lee, W. Yang and R. G. Parr, *Phys. Rev. B: Condens. Matter*, 1988, **37**, 785–789.

57 E. van Lenthe and E. J. Baerends, *J. Comput. Chem.*, 2003, **24**, 1142–1156.